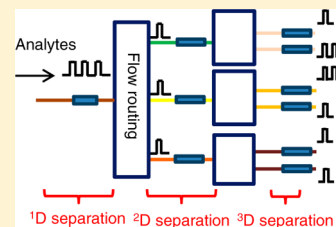


Smart Three-Dimensional Gas Chromatography

Di Chen,^{†,‡} Jung Hwan Seo,^{‡,§,⊥} Jing Liu,^{†,‡} Katsuo Kurabayashi,^{‡,§} and Xudong Fan^{*,†,‡}[†]Department of Biomedical Engineering, University of Michigan, 1101 Beal Avenue, Ann Arbor, Michigan 48109, United States[‡]Center for Wireless Integrated Microsensing and Systems, University of Michigan, 1301 Beal Avenue, Ann Arbor, Michigan 48109, United States[§]Department of Mechanical Engineering, University of Michigan, 2350 Hayward, Ann Arbor, Michigan, 48109, United States[⊥]Department of Mechanical and System Design Engineering, Hongik University, 94 Wausan-ro, Mapo-gu, Seoul, 121-791, South Korea

Supporting Information

ABSTRACT: We developed a complete computer-controlled smart 3-dimensional gas chromatography (3-D GC) system with an automation algorithm. This smart 3-D GC architecture enabled independent optimization of and control over each dimension of separation and allowed for much longer separation time for the second- and third-dimensional columns than the conventional comprehensive 3-D GC could normally achieve. Therefore, it can potentially be employed to construct a novel GC system that exploits the multidimensional separation capability to a greater extent. In this Article, we introduced the smart 3-D GC concept, described its operation, and demonstrated its feasibility by separating 22 vapor analytes.



Gas chromatography (GC) is one of the most effective methods for volatile organic compounds (VOCs) analysis and has been used in a broad range of applications. In order to further enhance the GC peak capacity, multidimensional GC is proposed and developed where each analyte is subject to multiple separations in multiple columns.^{1,2} In particular, comprehensive 2-dimensional GC (GC×GC) has been under intensive development in recent years. A typical GC×GC configuration has two separation columns connected in series with a thermal modulator installed in between.^{2,3} The modulator slices each single effluent peak from the first-dimensional (¹D) column into a series of smaller segments (usually on the order of sub- to several seconds) and sends them sequentially into the second-dimensional (²D) column. Despite its enhanced separation capability, the conventional GC×GC suffers severely from the conflicting requirement for a long ²D separation time needed for sufficient ²D separation and a short modulation cycle needed for better reconstruction of the ¹D separation. Usually, the ²D column is short in order to avoid the potential wrap-around issue.⁴ As such, the actual GC×GC peak capacity is far from the theoretical maximum $n_1 \times n_2$, where n_1 and n_2 are the peak capacities of the ¹D and ²D columns under optimal stand-alone conditions, respectively.^{4–8} In addition to GC×GC, comprehensive 3-dimensional gas chromatography (GC×GC×GC) has also been explored on the basis of the architecture similar to that in GC×GC.^{9–11} However, due to the aforementioned conflicting requirement, restrictions on the separation in the later stage become more stringent and detrimental. For example, while the maximally allowed ²D separation was 5 s, only 0.2 s was allowed in the ³D separation,^{10,11} significantly limiting the capability of GC×GC×GC.

We recently demonstrated smart multichannel 2-dimensional GC (2-D GC) architecture consisting of a flow-through on-column vapor detector and a flow routing module placed between ¹D and ²D columns, which allows for much longer ²D separation time without concern of the wrap-around issue in the conventional GC×GC.^{12,13} The ¹D and ²D retention times are directly measured by the ¹D and ²D vapor detectors installed right after the corresponding columns. Through this GC architecture, the separation processes in the two adjacent dimensions are “de-coupled” and can be optimized independently to fully exploit the multiplication of the peak capacity of each dimension. Furthermore, the architecture can be conveniently cascaded for higher dimensional separation.

In this Article, we aimed to capitalize on our previous work on the smart 2-D GC and develop smart 3-dimensional GC (3-D GC) architecture. A general configuration of the proposed multichannel 3-D GC system is illustrated in Figure 1A. The system consists of three sets of columns of different polarities representing three dimensions of separation. After each column, there is a flow-through on-column nondestructive vapor detector that can detect analytes without interference to analytes or flow.^{14–16} Between two neighboring dimensions, a flow routing module is installed to stop/continue the flow when needed and distribute the eluted analytes into different channels of the same dimension. The overall operation procedures are described as follows. The initial vapor mixture is first separated by the ¹D column into multiple peaks (clusters), each of which may contain multiple coeluted

Received: April 18, 2013

Accepted: June 21, 2013

Published: June 21, 2013

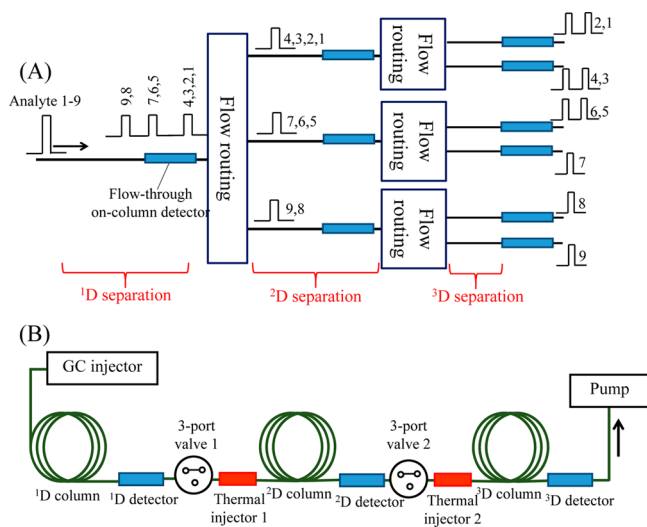


Figure 1. (A) Conceptual illustration of $1 \times 3 \times 6$ -channel 3-D GC architecture. The initial vapor mixture is first separated into multiple peaks (or clusters) by the ^1D column. Each peak, which may contain multiple coeluted analytes, is further separated by downstream higher-dimensional columns. Between two adjacent separation columns, a flow-through on-column vapor detector and a flow routing system work together to detect and route the vapor peaks from the upstream column and then inject them into the downstream column. (B) Schematic of a $1 \times 1 \times 1$ -channel 3-D GC system used in the experiment. ^1D , ^2D , and ^3D columns were Rtx-5 ms, Rtx-1, and SUPELCOWAX-10, respectively. They were 0.8, 1.0, and 3.0 m long, respectively, and had an inner diameter of $250 \mu\text{m}$. Vapor mixtures were initially injected using an injector on a commercial Varian 3000 GC instrument and then pulled through the entire system via a pump. Three home-built flow-through on-column vapor detectors and two home-built thermal injectors were used for vapor detection and injection. Helium was used as carrier gas.

analytes. When the entire peak is detected, it is loaded onto the thermal injector and injected into the downstream column for higher-dimensional separation. Multiple channels in each dimension are employed to accommodate multiple peaks coming from the upstream columns. In the present work, we implemented the above smart 3-D GC concept in a $1 \times 1 \times 1$ -channel fashion (see Figure 1B). We first built a complete computer-controlled 3-D GC system with an automation algorithm and then demonstrated its feasibility by analyzing 22 analytes.

EXPERIMENTAL SECTION

Materials. All the analytes used in the experiment were purchased from Sigma (St. Louis, MO) or Fisher Scientific (Pittsburgh, PA) and had purity greater than 97%. Rxi guard column (part no. 10029, i.d. = $250 \mu\text{m}$), Rtx-1 (part no. 10123, i.d. = $250 \mu\text{m}$), and Rtx-5 ms (part no. 12623, i.d. = $250 \mu\text{m}$) were purchased from Restek (Bellefonte, PA). SUPELCOWAX-10 capillary column and Carboxpack B adsorbent were purchased from Supelco (Bellefonte, PA). Universal quick seal column connectors (part no. 23627) and universal angled “Y” connectors (part no. 20403-261) were purchased from Sigma and Restek, respectively. Three-port valves (part no. 009-0269-900) and mini-diaphragm pumps (part no. D713-22-01) were purchased from Parker (Cleveland, OH). All materials were used as received.

Experimental Setup. The schematic of the smart 3-D GC is illustrated in Figure 1B. The main function block of the

system consisted of a commercial GC injector, one 0.8 m long Rtx-5 ms ^1D column with the ^1D flow-through on-column optical vapor detector installed at its end, one 1.0 m long Rtx-1 ^2D column with the corresponding ^2D vapor detector, and one 3.0 m long SUPELCOWAX-10 ^3D column with the corresponding ^3D vapor detector. The flow routing module between the two adjacent separations consisted of one three-port valve and one thermal injector. The details of the vapor detector, the three-port valve, and the thermal injector can be found in the Supporting Information.

The column polarity for each individual dimension was similar to what had been reported previously.^{10,11} The ^1D column was intermediate polar Rtx-5 ms. In the latter two dimensions, we adopted the conventional column selection in GC \times GC systems to reach a high degree of “orthogonality”.¹⁷ Therefore, nonpolar Rtx-1 and polar SUPELCOWAX-10 were chosen for the ^2D and ^3D columns, respectively. In order to fully demonstrate the advantages of the 3-D GC system while using the limited collections of testing analytes that we had, in this $1 \times 1 \times 1$ 3-D GC setup, we intentionally shortened the length of the ^1D and ^2D columns to limit their maximum separation capabilities so that the benefit of the 3-D separation could become more evident in the upcoming tests.

The analysis was conducted in an isothermal condition at room temperature. The analytes were prepared and mixed in a cleansed container and then sampled by a solid-phase microextraction (SPME) sampler and quickly injected into a Varian 3000 GC injector preheated to $250 \text{ }^\circ\text{C}$. The head pressure of the GC injector was set to zero. Gas analytes and ultrahigh purity (UHP) helium (used as carrier gas) were drawn into the system by the mini-diaphragm pump at a flow rate of approximately 6.5 mL/min. The entire operation was controlled by a computer with an in-house automation algorithm which controls the switching of valves based on peak detection from sensors adapted from our 2-D GC operation algorithm reported previously.¹³

Operation Procedures. Initially, all the columns were connected via the three-port valves. The analytes were injected through a GC injector. Then, the operation procedures consisted of three steps (Figure 2).

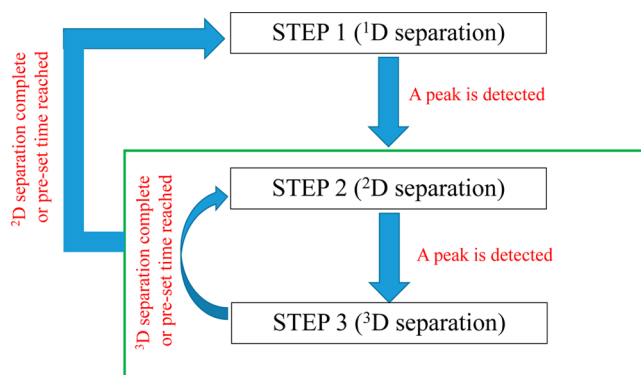


Figure 2. Flowchart of the operation procedures.

Step 1. The analytes underwent the ^1D separation. When an eluted peak, which might contain multiple coeluted analytes, passed the ^1D detector and was trapped by the first thermal injector, a control signal was sent to the first three-port valve to disconnect the ^1D and ^2D columns so that the subsequent separation in the ^1D column was suspended. Meanwhile, the

first thermal injector was turned on to reach up to 300 °C to inject the trapped analytes into the ²D column.

Step 2. This step is essentially the same as Step 1. The analytes underwent the ²D separation. When an eluted peak, which might contain multiple coeluted analytes, passed the ²D detector and was trapped by the second thermal injector, a control signal was sent to the second three-port valve to disconnect the ²D and ³D columns so that the subsequent separation in the ²D column was suspended (Note that the separation in the ¹D column was still suspended). Meanwhile, the second thermal injector was turned on to reach up to 300 °C to inject the trapped analytes into the ³D column.

Step 3. The analytes underwent the ³D separation. When all the analytes under the ³D separation were eluted or after a preset time interval (e.g., 5 min), the second three-port valve was reconnected to resume the ²D separation, and the subsequently eluted peaks from the ²D column were injected into the ³D column according to Step 2. When all the analytes under the ²D separation were eluted or after a preset time interval, the first three-port valve was reconnected to resume the ¹D separation according to Step 1.

RESULTS AND DISCUSSION

Figure 3 illustrates the details of how the smart 3-D GC system works by using four analytes, ethylene glycol monomethyl

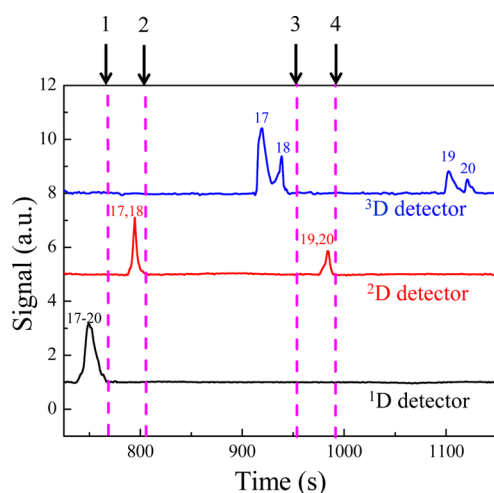


Figure 3. Example of three-dimensional separation using the system shown in Figure 1B. A peak formed by the four coeluted analytes (#17–#20) after the ¹D separation passed the ¹D detector and was loaded on Thermal injector 1. At 768 s (Arrow 1), this peak was injected into the ²D column. Then, the first peak was formed by the two coeluted analytes (#17 and #18) after the ²D separation passed the ²D detector and was loaded on the Thermal injector 2. At 808 s (Arrow 2), this peak was injected into the ³D column. At 955 s (Arrow 3), the ³D separation was complete. Next, the second peak on the ²D formed by the two coeluted analytes (#19 and #20) passed the ²D detector and was loaded on the Thermal injector 2. At 992 s (Arrow 4), this peak was injected into the ³D column. Curves are vertically shifted for clarity.

ether, chlorobenzene, ethylene glycol monoethyl ether, and isopropanol (Analyte #17–#20 in Table 1), as a model system. These four analytes were coeluted from the ¹D column, as represented by a single peak in the lower trace of Figure 3. After the entire peak was detected, it was injected into the ²D column at 768 s (Arrow 1 in Figure 3). The ²D separation yielded two coeluted peaks with the first peak containing

Table 1. Analytes Used in the Experiment

1	carbon disulfide
2	dichloroethylene
3	methyl <i>t</i> -butyl ether
4	dichloromethane
5	chloroform
6	hexane
7	dimethylformamide
8	benzene
9	carbon tetrachloride
10	trichloroethylene
11	dioxane
12	toluene
13	vinyl acetate
14	tetrachloroethylene
15	ethylbenzene
16	ethylene glycol
17	ethylene glycol monomethyl ether
18	chlorobenzene
19	ethylene glycol monoethyl ether
20	isopropanol
21	styrene
22	<i>m</i> -xylene

Analyte #17 and #18 and the second peak containing Analyte #19 and #20. At 808 s (Arrow 2), the first peak from the ²D column was injected into the ³D column, and meanwhile, the ²D separation was suspended. The ³D separation resulted in two well-resolved peaks representing Analyte #17 and #18, respectively. At 955 s (Arrow 3), the ³D separation was complete and the ²D separation was resumed. Then, the second peak was eluted out of the ²D column, and at 992 s (Arrow 4), this peak was injected into the ³D column, which resulted in two well-resolved peaks representing Analyte #19 and #20, respectively.

Analysis of 22 VOCs. After the illustration of the working principle of the smart 3-D GC system, we demonstrated complete separation of 22 analytes listed in Table 1. To highlight the capability of the smart 3-D GC, these analytes were intentionally selected so that some of them were coeluted at the ¹D and ²D separation. As shown in Figure 4, after the ¹D separation, 5 coeluted peaks emerged, which were further separated into 9 coeluted peaks after the ²D separation. Eventually, all analytes were separated after the ³D separation.

Retention Time Calculation and Chromatogram Construction. Each analyte undergoing this 3-D GC system has three retention times (¹*t*_R, ²*t*_R, and ³*t*_R) corresponding to three-dimensional separation, which can easily be extracted on the basis of the real-time chromatogram traces in Figure 4 using the following equation:

$$t_R = t_{\text{elute}} - \sum t_{\text{resume}} + \sum t_{\text{suspend}} - t_{\text{start}}$$

where *t*_{start} and *t*_{elute} are the time when analytes are injected and eluted out of a particular column, respectively. *t*_{suspend} and *t*_{resume} are the time when the separation is suspended and resumed, respectively. For example, to calculate the ²D retention time of ethylene glycol monoethyl ether (Analyte #19) shown in Figure 3, we used *t*_{start} = 768 s, *t*_{suspend} = 808 s, *t*_{resume} = 955 s, and *t*_{elute} = 984 s to obtain ²*t*_R = 69 s. Similarly, using *t*_{start} = 992 s and *t*_{elute} = 1102 s, we obtain ³*t*_R = 110 s for #19. Note that no separation suspension or resumption was conducted for the ³D separation for #19. Therefore, *t*_{suspend} = *t*_{resume} = 0 s.

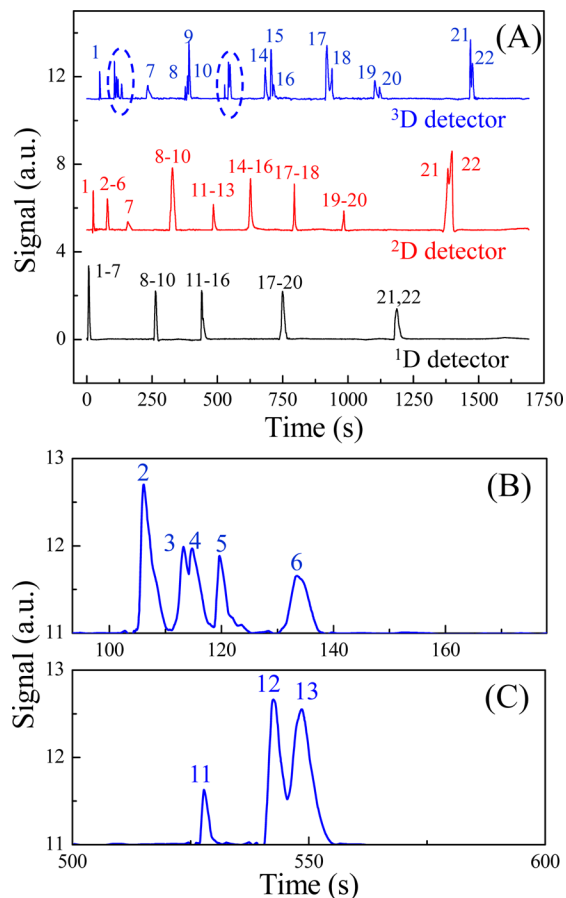


Figure 4. (A) Real-time chromatograms from the ^1D , ^2D , and ^3D detectors under isothermal conditions at room temperature. Curves are vertically shifted for clarity. Circled parts in the top curve are enlarged in (B) and (C), respectively.

With all 3-D retention times acquired, it is then straightforward to construct the 3-D chromatogram as shown in Figure 5A. A 2-D chromatogram can easily be formed by projecting the 3-D chromatogram onto any 2-D space, as exemplified in Figure 5B. Note that over 100 s of ^2D and ^3D

separation was used in our 3-D GC system to separate those 22 analytes, which was otherwise very difficult to accomplish with the conventional GC×GC or GC×GC×GC architecture. Note that, due to the additive (or scalable) nature of the smart GC architecture, the above 3-D GC system can also be interpreted as a “pre-separation” stage (i.e., the ^1D separation), followed by a smart 2-D GC subsystem. With this “pre-separation” stage, analytes are regrouped before entering the 2-D GC subsystem and each group may contain far fewer analytes than originally in the vapor mixture, which can significantly lessen the separation burden on the downstream 2-D GC subsystem and improve its performance.

CONCLUSION AND FUTURE WORK

We have built a complete smart 3-D GC system that allows for independent control over each dimension of separation and much longer separation time for higher dimensions, thus providing a platform for us to fully exploit the power of the multidimensional GC. Future work will be to adapt the smart 3-D GC to develop smart 3-D micro-GC where multidimensional separation provides the much needed high peak capacity. Multiple channels will also be implemented to shorten the overall analysis time. In addition, a hybrid system, which was previously demonstrated in a different configuration,¹⁸ will be explored that includes a “pre-separation” stage and a conventional GC×GC (or micro-GC×GC) subsystem. Furthermore, the temperature ramping method can be implemented to expedite the analysis time, as shown in our previous work.¹³ Finally, we note that our current demonstration required baseline separation in each column so that the algorithm was able to decide a peak. In practice, baseline separation may not be achieved. A possible solution may be a “cut and stitch” method that involves multiple columns in the same dimension. Another possible solution may be to treat the ^1D separation as the sample preparation stage as discussed earlier. Complex samples will be pre-separated into simpler groups, each of which will then be subjected to 2-D separation. In the future, this issue needs to be addressed before the proposed smart 3-D GC becomes practically useful.

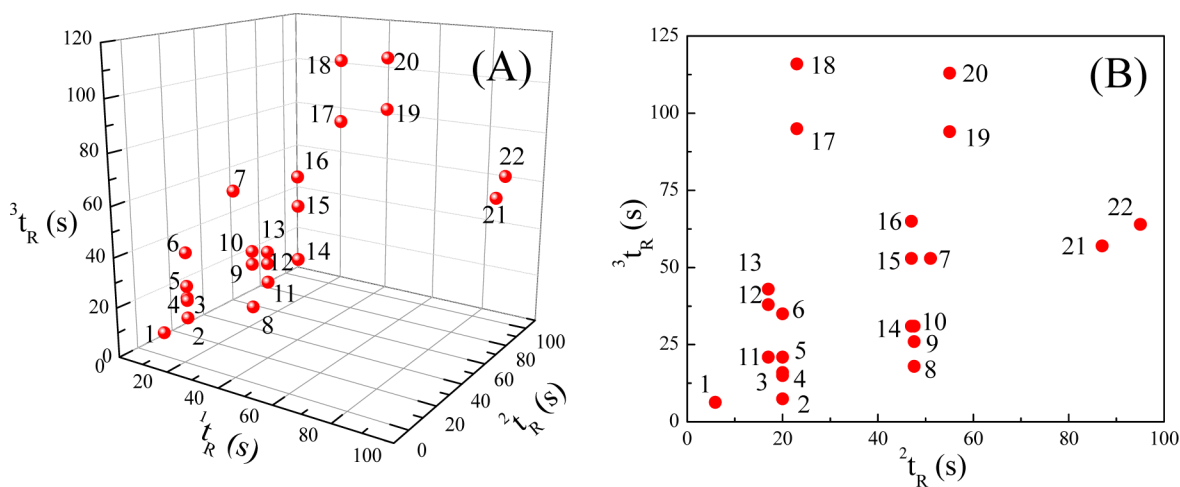


Figure 5. (A) 3-D chromatogram extracted from Figure 3. (B) 2-D display of the ^2D and ^3D retention time of the 3-D chromatogram in (A). The retention time of a peak in each dimension is measured at its apex. Details of the retention time for each analyte are listed in Table S1, Supporting Information.

■ ASSOCIATED CONTENT

📄 Supporting Information

Additional information as noted in the text. This material is available free of charge via the Internet at <http://pubs.acs.org>.

■ AUTHOR INFORMATION

Corresponding Author

*E-mail: xsfan@umich.edu.

Notes

The authors declare no competing financial interest.

■ ACKNOWLEDGMENTS

We would like to thank the National Science Foundation (IOS-0946735) for the financial support.

■ REFERENCES

- (1) Beens, J.; Boelens, H.; Tijssen, R.; Blomberg, J. J. *High Resolut. Chromatogr.* **1998**, *21*, 47–54.
- (2) Seeley, J. V.; Seeley, S. K. *Anal. Chem.* **2012**, *85*, 557–578.
- (3) Liu, Z. J. *Chromatogr., A* **1991**, *29*, 227–231.
- (4) Serrano, G.; Dibyadeep, P.; Kim, S.-J.; Kurabayashi, K.; Zellers, E. *T. Anal. Chem.* **2012**, *84*, 6973–6980.
- (5) Seeley, J. V. *J. Chromatogr., A* **2012**, *1255*, 24–37.
- (6) Blumberg, L. M.; David, F.; Klee, M. S.; Sandra, P. *J. Chromatogr., A* **2008**, *1188*, 2–16.
- (7) Oldridge, N.; Panic, O.; Górecki, T. *J. Sep. Sci.* **2008**, *31*, 3375–3384.
- (8) Meinert, C.; Meierhenrich, U. J. *Angew. Chem., Int. Ed.* **2012**, *51*, 10460–10470.
- (9) Ledford, E. B. J.; Billesbach, C. A.; Zhu, Q. *J. High Resolut. Chromatogr.* **2000**, *23*, 205–207.
- (10) Watson, N. E.; Siegler, W. C.; Hoggard, J. C.; Synovec, R. E. *Anal. Chem.* **2007**, *79*, 8270–8280.
- (11) Siegler, W. C.; Crank, J. A.; Armstrong, D. W.; Synovec, R. E. *J. Chromatogr., A* **2010**, *1217*, 3144–3149.
- (12) Liu, J.; Khaing Oo, M. K.; Reddy, K.; Gianchandani, Y. B.; Schultz, J. C.; Appel, H. M.; Fan, X. *Anal. Chem.* **2012**, *84*, 4214–4220.
- (13) Liu, J.; Seo, J. H.; Li, Y.; Chen, D.; Kurabayashi, K.; Fan, X. *Lab Chip* **2013**, *13*, 818–825.
- (14) Shopova, S. I.; White, I. M.; Sun, Y.; Zhu, H.; Fan, X.; Frye-Mason, G.; Thompson, A.; Ja, S.-j. *Anal. Chem.* **2008**, *80*, 2232–2238.
- (15) Sun, Y.; Liu, J.; Howard, D. J.; Fan, X.; Frye-Mason, G.; Ja, S.-j.; Thompson, A. K. *Analyst* **2010**, *135*, 165–171.
- (16) Liu, J.; Sun, Y.; Howard, D. J.; Frye-Mason, G.; Thompson, A. K.; Ja, S.-j.; Wang, S.-K.; Bai, M.; Taub, H.; Almasri, M.; Fan, X. *Anal. Chem.* **2010**, *82*, 4370–4375.
- (17) Omais, B.; Courtiade, M.; Charon, N.; Ponthus, J.; Thiébaud, D. *Anal. Chem.* **2011**, *83*, 7550–7554.
- (18) Mitrevski, B.; Marriott, P. J. *Anal. Chem.* **2012**, *84*, 4837–4843.